Plant Soil (2019) 444:299–314
https://doi.org/10.1007/s11104-019-04283-8

REGULAR ARTICLE

Transcriptome analysis of *Medicago lupulina* seedlings leaves treated by high calcium provides insights into calcium oxalate formation

Xi-Min Zhang · Lun-Xian Liu · Zhi-Meng Su · Zhi-Jun Shen · Gui-Feng Gao · Yin Yi · Hai-Lei Zheng

Received: 2 April 2019 / Accepted: 23 August 2019 / Published online: 29 August 2019

Abstract

Background and aim Calcium oxalate (CaOx) is a common biomineral found in the plant kingdom. Crystals of CaOx occur in different plant tissues, such as leaves and stems. However, little is known about the biosynthesis of CaOx in oxalate-accumulating plants. Moreover, the literature on genes related to CaOx formation under high-calcium environment is scarce. In the present study, the physiological parameters and the transcript profiles of *Medicago lupulina* leaves treated with 0.1 and 25 mM Ca^{2+} were analyzed to study the genes involved in the biosynthesis of CaOx.

Results We demonstrated that exposure to high external calcium concentration induced H_2O_2 production, ascorbic acid degradation, and CaOx accumulation in *M. lupulina* leaves. Moreover, we identified 1715 differentially expressed genes (DEGs) (1322 up-regulated and 393 down-regulated genes) in leaves treated with 25 mM Ca^{2+} compared with the leaves treated with 0.1 mM Ca^{2+}. We further demonstrated the involvement of DEGs in oxalic acid production, calcium transport, and calcium buffering. These results revealed that a high calcium promoted oxalic acid biosynthesis by inducing the expression of NADPH oxidase and ascorbate oxidase genes. In addition, several genes encoding cyclic nucleotide-gated channel, Ca^{2+}-ATPase, H^+/Ca^{2+} exchangers, and calcium-binding proteins were found to be differentially expressed and involved in calcium transport and calcium buffering.

Conclusion Our transcriptome analyses provide a comprehensive insight into the biosynthesis of CaOx in oxalate-accumulating plants.

Keywords Calcium oxalate · High calcium · *Medicago* · Oxalate-accumulating plants · Transcriptome

Responsible Editor: Honghua He.

Electronic supplementary material The online version of this article (https://doi.org/10.1007/s11104-019-04283-8) contains supplementary material, which is available to authorized users.

X.-M. Zhang · Z.-J. Shen · G.-F. Gao · H.-L. Zheng (✉)
Key Laboratory for Subtropical Wetland Ecosystem Research of MOE, College of the Environment and Ecology, Xiamen University, South Xiangan Road, Xiangan District, Xiamen, Fujian 361102, People's Republic of China
e-mail: zhenghl@xmu.edu.cn

X.-M. Zhang
e-mail: zhxm409@163.com

Z.-J. Shen
e-mail: shenzj1987@stu.xmu.edu.cn

G.-F. Gao
e-mail: gfgao1989@stu.xmu.edu.cn

Introduction

Calcium oxalate (CaOx) crystals are extensively distributed in higher plants (Franceschi and Nakata 2005; Horner et al. 2012; Lersten and Horner 2009; Nakata 2003; Webb 1999). These are primarily synthesized in the vacuoles of specialized crystal-forming cells or vein

cells (Franceschi 2001; Franceschi and Nakata 2005). Although not all plants contain CaOx crystals, such as *Arabidopsis* (Nakata 2012), their abundance in the plant could be understood from the fact that CaOx could account for 3–80% of dry weight in some organs (Libert and Franceschi 1987) and greater than 90% of overall calcium content (Gallaher 1975) of oxalate-accumulating plants. The CaOx crystals in plants exhibit several important physiological functions, including heavy metal detoxification, light regulation, pollen release, resistance to plant pathogens and pest infestation, contribution to biogeochemical cycles of carbon and calcium, calcium homeostasis, and photosynthesis (Franceschi 2001; He et al. 2014; Pierantoni et al. 2018; Tooulakou et al. 2016).

Although CaOx crystals are widely present in the plants, little is known about their biosynthesis and regulation of production of oxalic acid. Under normal conditions, the concentration of oxalic acid is usually low in oxalate non-accumulating plants (Nuss and Loewus 1978). However, a high soil calcium level could induce excessive accumulation of oxalic acid in oxalate-accumulating plants (Franceschi 1989; Mazen et al. 2004; Volk et al. 2002). The formation of CaOx crystals under such conditions is recognized as a detoxification mechanism to lower excessive free oxalic acid (Franceschi and Nakata 2005; He et al. 2014). Numerous precursors for oxalic acid biosynthesis have been proposed, including isocitrate, oxaloacetate, glycolate/glyoxylate, and L-ascorbic acid (Yu et al. 2010). Of these, the oxidative cleavage of L-ascorbic acid is considered to be the most effective for the formation of CaOx crystals (Horner et al. 2000; Horner and Wagner 1995; Keates et al. 2000; Kostman et al. 2001; Truffault et al. 2016) as compared with other precursors such as glycolate (Kausch and Horner 1985). In cell-suspension cultures of *Rosa*, ascorbic acid (AsA) was enzymatically hydrolyzed in the presence of exogenous H_2O_2 to form oxalic acid by an unknown enzyme (Green and Fry 2005; Parsons and Fry 2012; Parsons et al. 2011; Truffault et al. 2016).

The formation of CaOx crystal requires the cross-membrane transport of calcium into the vacuoles from the cytoplasm, endoplasmic reticulum (ER), or mitochondria. In the crystal idioblasts, calcium uptake from the apoplasts is regulated by calcium channels owing to the existence of an electrochemical potential gradient for Ca^{2+} between the endomembranes (Franceschi and Nakata 2005; Volk et al. 2004). A study has confirmed the involvement of dihydropyridine-type Ca^{2+} channels in the formation CaOx crystal through calcium channel blockers (Volk et al. 2004). However, further studies are warranted to identify the calcium channels related to the biosynthesis of CaOx crystal.

It has been reported that the nucleation and growth of CaOx crystals in the vacuoles are regulated by several biomacromolecules, such as crystal matrix protein, polysaccharides, lipids, calcium-binding proteins (CBPs), and calsequestrin (Franceschi et al. 1993; Li et al. 2003; Webb 1999; Webb et al. 1995). Additionally, the formation of CaOx crystal is extremely rapid (Franceschi 1989) and shape and size of crystals are constant within the vacuoles (Franceschi and Nakata 2005). Therefore, the formation of CaOx crystals is believed to be highly regulated by several genetic factors rather than a simple precipitation process (Nakata and Mcconn 2000). For example, some reports have confirmed the involvement of more than one gene in the formation of CaOx crystals using calcium oxalate defective mutants of *Medicago truncatula* (Mcconn and Nakata 2002; Nakata and Mcconn 2000; Nakata and Mcconn 2003). In addition, Li et al. (2003) suggested the involvement of two regulatory steps in CaOx formation. The first step is the buffering of the cytosolic calcium by calreticulin localized in the specialized ER in the idioblasts. The other step is that CaOx precipitation within the vacuoles could be controlled by several biomacromolecules. However, these details need to be validated by further studies.

Medicago lupulina, an annual herbaceous legume with high CaOx levels, is widely grown in high-calcium environments. This is attributed to its extremely high tolerance to increased soil calcium levels. It serves as an ideal plant model to study the molecular

X.-M. Zhang · L.-X. Liu · Z.-M. Su · Y. Yi (✉)
Key Laboratory of State Forestry Administration on Biodiversity Conservation in Karst Area of Southwest, Guizhou Normal University, No. 116 Baoshan Road (N), Guiyang, Guizhou 550001, People's Republic of China
e-mail: gzklppdr@gznu.edu.cn

L.-X. Liu
e-mail: 315297850@qq.com

Z.-M. Su
e-mail: 1843455301@qq.com

mechanisms of high calcium-induced CaOx formation. Although the biological functions of CaOx crystals in plants have been studied recently, the genes involved in their formation, calcium transport, CaOx nucleation, and oxalic acid biosynthesis have not been reported in legumes under high external calcium conditions. Recently, the studies at the transcriptional level have revealed the genes related to CaOx formation in animals (Okada et al. 2010; Joshi et al. 2013; Joshi et al. 2017). However, so far, the transcriptome method has not been employed to identify the relevant genes involved in the biosynthesis of CaOx in plants, and specifically in *M. lupulina*, an oxalate-accumulating plant. Therefore, the objective of the present study is to reveal the genes involved in the biosynthesis of CaOx in plants using transcriptome analysis.

Materials and methods

Plant growth, and calcium and drought treatment

The *M. lupulina* seeds were soaked in concentrated sulfuric acid for 7 min, followed by three washes with distilled water. The seeds were then planted in a plastic pot containing perlite with 1/4 MS solution in hydroponics. They were cultured in a chamber with 16/8 h light/dark at 22 °C /20 °C, irradiance of 350 μmol m^{-2} s^{-1} and air relative humidity of 60 to 70%. After culturing for 30 days, the culture solution was replaced with a new 1/4 MS solution modified by 0.1 and 25 mM $CaCl_2$. Subsequently, the seedlings were treated for another ten days. Finally, the treated roots, stems, and leaves were collected to measure CaOx. The treated leaves were also collected for RNA sequencing and assessing the physiological parameters.

Determination of oxalate and ascorbate content

The root, stem and leaf samples were extracted in 2 mL of deionized water and 2 M HCl to obtain soluble and total oxalate, respectively. Insoluble oxalate was calculated by subtracting the soluble oxalate from the total oxalate. According to Nakata and Mcconn (2000), insoluble oxalate content represents CaOx content. The mixtures were centrifuged at 10,000×*g* for 10 min at 4 °C. The supernatant was collected and quantified using a series Agilent 1200 HPLC system (www.agilent.com, Santa Clara, USA) with an injection volume 10 μL. The absorbance was measured at 215 nm. A Carbomix H-NP 10:8%, 7.8 × 50 mm, 10 μm with a security guard column at 55 °C (www.sepax-tech.com, Delaware, USA) was used with 0.1% phosphoric acid at a flow rate of 0.6 mL min^{-1}. A calibration curve based on the elution profiles of the oxalic acid standard was used to estimate the sample concentrations (Minocha et al. 2015). Reduced and oxidized ascorbate contents in the treated leaves were measured using the Gillespie method (Km and Ea 2007).

Determination of hydrogen peroxide content and DAB staining

Hydrogen peroxide (H_2O_2) contents in the treated leaves were determined according to the method described by Bafeel and Ibrahim (2008). The 3,3′-diaminobenzidine (DAB) staining was performed as per the method described by Daudi et al. (2012).

Observation of CaOx distribution and morphology

The fresh treated leaf samples (treated for ten days) were decolored using 2 mL of 2.5% sodium hypochlorite solution. The images were obtained using an optical microscope (LM) (Eclipse 80i, www.nikon.com, Tokyo, Japan). The treated leaf epidermis was dehydrated and observed to study the morphology of CaOx crystals with a scanning electron microscope (SEM) (S-4800, www.hitachi.com, Tokyo, Japan).

Determining the density and length of CaOx crytals

The density and length of CaOx crystals were calculated from the obtained images using the Photoshop software (www.xitongtiandi.net).

XRD and FTIR spectra

The powder spectra of all treated leaves were analyzed using the X-ray diffraction (XRD) (XPert, www.malvernpanalytical.com.cn, Alemlo, Holland). Fourier transform infrared (FTIR) spectroscopy was used to record the infrared spectrum of samples on a spectrometer (Nicolet iS5, www.thermofisher.com, Waltham, USA) at a resolution of 4 cm^{-1}.

RNA extraction, cDNA library construction, and Illumina deep sequencing

The leaves of seedlings treated with 0.1 and 25 mM Ca^{2+} for ten days were collected. Total RNA was extracted from the sample using Trizol reagent (www.thermofisher.com, Carlsbad, CA, USA). Agarose gel electrophoresis (1%) was used to determine RNA degradation and contamination. The purity of RNA was checked using the NanoPhotometer spectrophotometer (www.implen.de, Munich, Germany). The RNA concentration was measured using the Qubit RNA Assay Kit in Qubit 2.0 Fluorometer (www.thermofisher.com, USA). The RNA integrity was assessed using the RNA Nano 6000 Assay Kit of the Agilent Bioanalyzer 2100 system (www.agilent.com, CA, USA). The sequencing libraries were constructed using the NEBNext Ultra RNA Library Prep Kit for Illumina (www.international.neb.com, USA) following the manufacturer's recommendations. The library preparations were sequenced on an Illumina HiSeq 2000 platform and paired-end reads were generated. Each sample yielded more than 6 Gb of clean data. Sequencing was completed by the Beijing Biomarker Biotechnology Company (www.biomarker.com.cn, China). The RNA sequence data of 0.1 and 25 mM $CaCl_2$-treated leaves were obtained in three biological replicates and leaves of 10 to15 seedlings were used in each replicate for RNA extraction. The sequences used in this study are listed in Supplementary Table S4.

Transcriptome assembly and detection of differentially expressed genes (DEGs)

Trinity method was utilized to accomplish the transcriptome assembly (Grabherr et al. 2011) with min_kmer_cov set to 2 by default and all other parameters set to default. The Fragments Per Kilobase of transcript per Million mapped reads (FPKM) method was used to calculate the unigene expression (Trapnell et al. 2010). The clean reads of each library were mapped to the sequences of each unigene. The significance of DEGs in 0.1 mM and 25 mM Ca^{2+}-treated leaves was determined using the DESeq R package (1.10.1). False discovery rate (FDR) was applied to identify the threshold of the p value in multiple tests. Genes were considered as differentially expressed when FDR was less than 0.01 and log ratio was greater than 1 (two-fold change) between the samples. In addition, t-test ($p < 0.05$) also assigned the gene as differentially expressed.

Annotation and classification of the differentially expressed genes

The differentially expressed gene functions were annotated based on the NCBI non-redundant database (Pruitt et al. 2005), COG (Tatusov et al. 2000), GO (Ashburner et al. 2000) and KEGG (Minoru et al. 2004) using BLAST with an E-value ≦ 1e–10 as the cutoff.

Phylogenetic analysis

The genes of *M. lupulina* were used to identify open reading frames (ORFs) and protein sequences using an ORF finder online tool (www.ncbi.nlm.nih.gov/orffinder/). The sequences of *Arabidopsis* were also obtained from the Arabidopsis Information Resource (www.arabidopsis.org) and subjected to phylogenetic analysis. Trees were constructed using the neighbour-joining method as implemented in the ClustalW program. Following parameters were set during the construction of the phylogenetic tree: substitution, Poisson's model, complete deletion, replication, and bootstrap analysis with 1000 replicates.

Quantitative real-time PCR analysis

Some annotated putative unigenes related to CaOx production or other genes were selected for quantitative real-time PCR (qRT-PCR) to verify RNA-Seq. The total RNA was extracted from the samples using the OmniPlant RNA Kit (www.cwbiotech.com, China) and was reverse-transcripted using the TransScript All-in-One First-Strand cDNA Synthesis SuperMix for qPCR Kit (www.transgen.com.cn, China) following the manufacturer's protocol. The primer sequences used for qRT-PCR are listed in Supplementary Table S3. *β-actin* was used as an internal control (Sun et al. 2014). qRT-PCR was performed using a Rotor-Gene Q real-time PCR system (www.qiagen.com/cn, Germany). A total of 10 μL 2 X TransStart Top/Tip Green qPCR SuperMix (www.transgen.com.cn, China) was added to the reaction according to the manufacturer's instructions. The relative expression levels of the selected genes normalized to the expression level of the *β-actin* gene were calculated

from cycle threshold values using the $2^{-\Delta\Delta Ct}$ method (Livak and Schmittgen 2012).

Statistical analysis

Data are expressed as mean ± standard deviation (SD) and were subjected to a one-way analysis of variance (ANOVA) or Student's two-tailed *t*-test. Analysis was carried out in at least three replicates for each sample and a value of $p < 0.05$ was considered to be statistically significant. All tests were performed using SPSS 18.0 for Windows (www.spss.com.hk, USA).

Results

High calcium induces CaOx crystal formation in *M. lupulina* leaves

We did not observe significant change in the CaOx content in the root and stem tissues between 0.1 and 25 mM Ca^{2+} treatments (Supplementary Fig. S1), whereas the levels of CaOx in the leaves treated with 25 mM Ca^{2+} for ten days increased significantly (Fig. 1a). In addition, there existed no significant change in crystal densities in leaves treated with 0.1 and 25 mM Ca^{2+} (Fig. 1b). However, the crystal length in leaves treated with 25 mM Ca^{2+} for ten days increased significantly (Fig. 1c). Moreover, SEM revealed prismatic CaOx crystals (Fig. 1d) and LM revealed a distribution of CaOx crystals in *M. lupulina* leaves along with the leaf vascular bundles (VBs) (Fig. 1e–h). The FTIR spectroscopy and XRD confirmed the crystals in *M. lupulina* leaves to mainly comprise CaOx (Supplementary Fig. S2).

RNA sequencing, de novo assembly and analysis of differentially expressed genes (DEGs)

In order to determine the expression pattern of genes related to CaOx biosynthesis pathways, the transcriptome data were obtained from the leaves of *M. lupulina* treated with 0.1 and 25 mM Ca^{2+} for ten days. We obtained a total of 31,145,156 clean reads from 0.1 mM Ca^{2+}-treated leaves and 31,806,752 clean reads from 25 mM Ca^{2+}-treated leaves. The total mapped reads in 0.1 and 25 mM Ca^{2+} samples accounted for 83.87% and 80.06% of the total clean reads, respectively (Table 1). The average GC content and Q20 were higher than 42.02% and 95.21%, respectively (Supplementary Table S1). After assembling the high-quality reads, a total of 85,389 unigenes were obtained with an average length of 775 bp. A majority of the unigenes had lengths less than 1000 bp and accounted for 77% of all unigenes. The length distribution of the unigenes is listed in Supplementary Table S2. A total of 1715 DEGs between 0.1 and 25 mM Ca^{2+} treatments are shown in Supplementary Fig. S3. In total, 1322 genes were found to be up-regulated and 393 genes down-regulated.

Gene expressions verified through real-time qRT-PCR

In order to verify the effectiveness of the transcriptome data, qRT-PCR was performed for eight genes selected from the transcriptome data. All qRT-PCR primers are listed in Supplementary Table S3. These selected genes were involved in calcium transport and biosynthesis of oxalic acid. The obtained qRT-PCR results correlated well with the transcriptome sequencing results (Fig. 2), suggesting that transcriptome data were accurate with high quality.

Functional classification of DEGs by gene ontology

The gene ontology (GO) classification analysis categorized 1715 DEGs into three functional ontologies, including biological process, cell components, and molecular functions (Fig. 3). Each unigene was allotted at least one GO term and a total of 29 level–2 GO terms were obtained from 1715 unigenes, including 13 for biological processes, 9 for cell components, and 7 for molecular functions. In the biological process category, the main unigenes were found to be involved in the metabolic processes (712 unigenes), cellular processes (570 unigenes), and single-organism processes (501 unigenes). For cell components, the top three groups were cells (306 unigenes), cell parts (306 unigenes), and membranes (242 unigenes). The top three represented groups in the molecular function included catalytic activity (613 unigenes), binding (565 unigenes), and transporter activity (91 unigenes) (Fig. 3).

Functional classification of differentially expressed genes by clusters of orthologous groups

All DEGs were annotated into the Clusters of Orthologous Groups (COG) database and mapped by

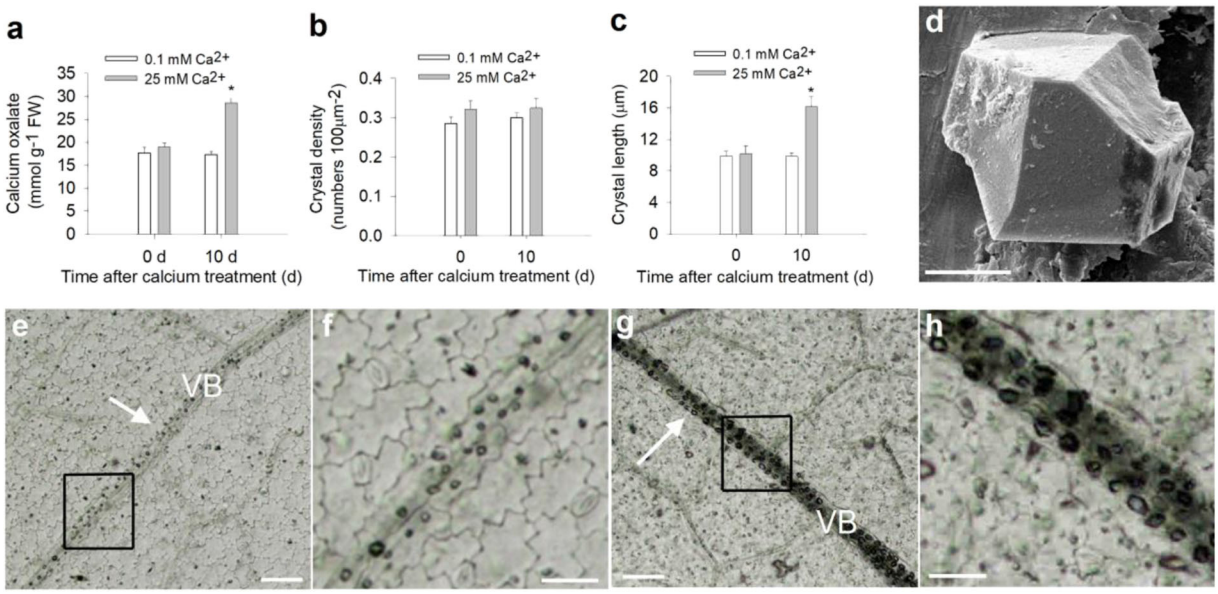

Fig. 1 Content, morphology and distribution of CaOx in *M. lupulina* leaf. a Content of calcium oxalate in leaf treated by 0.1 mM Ca^{2+} and 25 mM Ca^{2+} for 0 day and 10 days, respectively. **b** Crystal density in leaf vascular bundles treated by 0.1 mM Ca^{2+} and 25 mM Ca^{2+} for 0 day and 10 days, respectively. **c** Crystal length in leaf vascular bundles treated by 0.1 mM Ca^{2+} and 25 mM Ca^{2+} for 0 day and 10 days, respectively. Data are mean ± standard deviation (SD) of three replicates and asterisk represents a significant difference between 0.1 mM Ca^{2+} and 25 mM Ca^{2+} treatment ($p < 0.05$). **d** Prismatic crystals observed by scanning electron microscope (SEM), bar = 2 μm. **e-h** Distribution of calcium oxalate crystals (white arrows) along the leaf vascular bundles (VB) observed by optical microscope. **e** 0.1 mM Ca^{2+} treated leaf; **(f)** Amplification of the black box in **e**; **g** 25 mM Ca^{2+} treated leaf; **h** Amplification of the black box in **(g)**, bars = 40 μm

23 COG categories. Among them, the cluster of "general function prediction only" represented the largest functional group, followed by "signal transduction mechanisms", "replication, recombination and repair", "transcription" and "post-translational modification, protein turnover, chaperones". The categories "nuclear structure" and "extracellular structures" had no corresponding genes (Supplementary Fig. S4).

Functional classification of differentially expressed genes by Kyoto encyclopedia of genes and genomes

A total of 294 DEGs were also annotated into the Kyoto Encyclopedia of Genes and Genomes (KEGG) database for potential biological pathways represented in the *M. lupulina* transcriptome. In the present study, the annotated DEGs were divided into 99 pathways

Table 1 Summary of transcriptome reads mapped to the reference genome. The leaves of seedlings treated with 0.1 and 25 mM Ca^{2+} for 10 days were collected for RNA-seq. Data were analyzed using bioinformatics software described in Materials and Methods

Reads mapping	0.1 mM Ca^{2+}		25 mM Ca^{2+}	
	Number of reads	Percentage (%)	Number of reads	Percentage (%)
Total clean reads	31,145,156	100	31,806,752	100
Total base pairs	4,595,748,756	100	4,684,410,062	100
Unique match	19,736,269	75.56	18,853,771	74.04
Multi-position match	6,385,287	24.44	6,611,015	25.96
Total mapped reads	26,121,556	83.87	25,464,786	80.06
Total unmapped reads	5,023,600	16.13	6,341,966	19.94

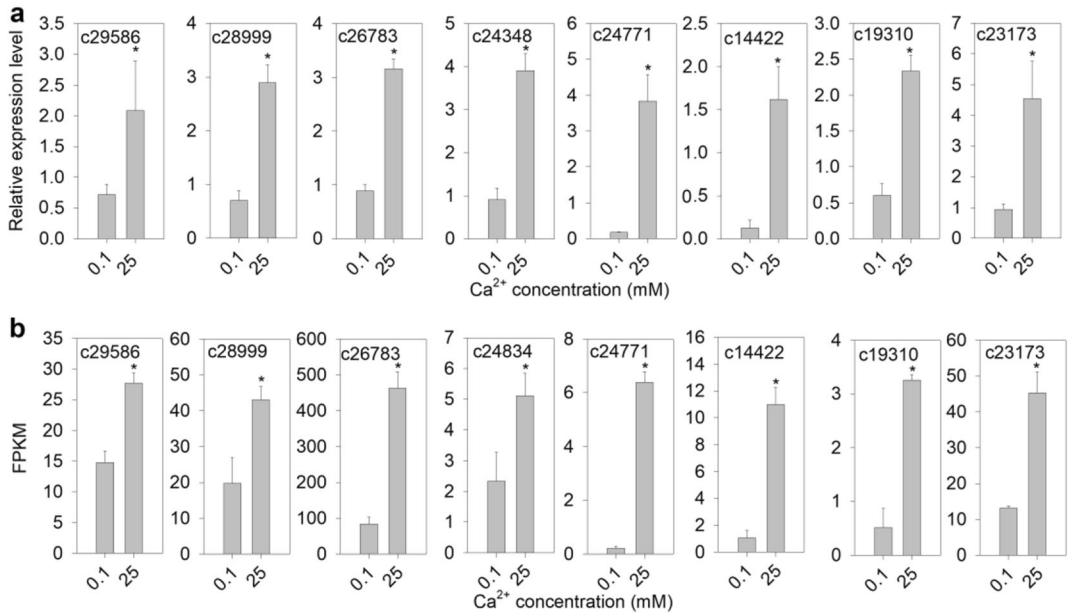

Fig. 2 Validation of putative unigenes from RNA-seq results using qRT-PCR. a Relative expression levels of 8 DEGs used in this study were detected using qRT-PCR under 0.1 and 25 mM Ca^{2+} treatment for 10 days. The relative expression levels of the selected genes normalized to the expression level of *β-actin* gene were calculated from cycle threshold values using the $2^{-\Delta\Delta Ct}$ method. **b** FPKM values of the selected genes were analyzed under 0.1 and 25 mM Ca^{2+} treatment for 10 days. Data are mean ± standard deviation (SD) of three replicates and asterisk represents a significant difference between 0.1 mM Ca^{2+} and 25 mM Ca^{2+} treatment ($p < 0.05$)

(Fig. 4). A large number of DEGs were mapped to categories, such as "phenylpropanoids biosynthesis", "plant-pathogen interaction" and "starch and sucrose metabolism", which may be involved in the oxalate biosynthesis. In addition, several DEGs were mapped to categories of "biosynthesis of amino acids" and "protein processing in endoplasmic reticulum", which may be involved transmembrane transport. Some DEGs that related to "plant hormone signal transduction" pathway played important roles in abiotic stress response (Fig. 4).

Genes related to ascorbic acid degradation in *M. lupulina* leaves under high-calcium treatment

Ascorbic acid (AsA) and dehydroascorbic acid (DHA) levels were measured to determine whether these correlated with the accumulation of insoluble oxalic acid under high calcium. We observed that the content of leaf AsA decreased, whereas DHA showed no significant changes after 10-day treatment with 25 mM Ca^{2+} (Fig. 5a and b). However, the insoluble oxalic acid content of leaves, represented by CaOx, increased significantly after 25 mM Ca^{2+} treatment (Fig. 1a), indicating that high calcium could induce AsA degradation and oxalic acid accumulation in *M. lupulina* leaves.

In plants, both ascorbate peroxidase (APX, EC:1.11.1.11) and ascorbate oxidase (AO, EC:1.10.3.3) are considered to be involved in the degradation of AsA (Parsons and Fry 2012; Parsons et al. 2011; Pignocchi et al. 2006). To determine which oxidase participated in oxalic acid biosynthesis, we successfully identified four genes encoding APX and two genes encoding AO from the transcriptome data. Among these, *c24348* encoding a cell wall-localized AO was found to be significantly up-regulated in 25 mM Ca^{2+} treated leaves, but not APX (Fig. 5c), indicating that the cell wall-localized AO rather than APX dominated the AsA oxidation to form DHA.

Genes related to H_2O_2 production in *M. lupulina* leaves under high-calcium treatment

In order to determine if a high calcium resulted in H_2O_2 accumulation in *M. lupulina* leaves, we tested the content of H_2O_2 using both biochemical assay and DAB staining method in 0.1 and 25 mM Ca^{2+}-treated leaves. A high accumulation of H_2O_2 in 25 mM Ca^{2+} treated leaves was

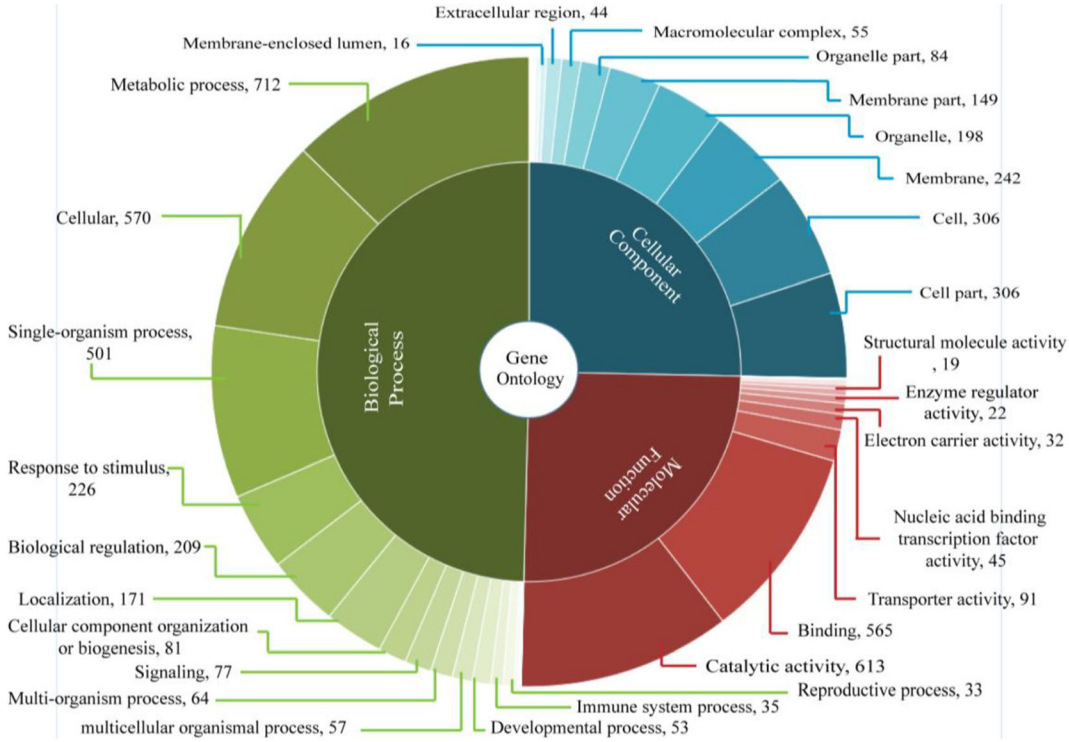

Fig. 3 Histogram presentation of Gene Ontology (GO) classification of DEGs. The results are summarized as three main categories: Biological Processes, Cellular Components and Molecular Functions. Number indicate the numbers of DEGs

found by biochemical assay (Fig. 5d) and DAB staining (Fig. 5e). In addition, four genes encoding NADPH oxidases (EC:1.6.3.1) (respiratory burst oxidase homologues [Rboh]), known to be involved in H_2O_2 accumulation, were identified by RNA sequencing. Among these, the expression of *c21327* was up-regulated, whereas other genes reported insignificant changes in their expression in the leaves exposed to high calcium for ten days (Fig. 5f). Furthermore, the phylogenetic analysis revealed that *c21327* is homologous with *AtRbohF* in *Arabidopsis* (Supplementary Fig. S5). These results indicated that the accumulation of H_2O_2 was induced by enhanced expression of *RbohF* gene in *M. lupulina* under high calcium.

Genes related to calcium transport and calcium binding proteins in high calcium-treated leaves

Another determinant factor of controlling CaOx formation is leaf calcium level that was further analyzed in the present study. Higher calcium content around 4.78 mg/g FW was found in 25 mM Ca^{2+}-treated leaves as compared with 0.1 mM Ca^{2+}-treatment in which only 0.08 mg/g FW was recorded (Fig. 6a). In addition, from transcriptome data, we found a group of genes related to calcium transport. Firstly, six genes encoding cyclic nucleotide-gated calcium channel (*CNGC*) were identified. Among these, the expression of *c8828* and *c23173* were significantly up-regulated under high calcium levels (Fig. 6b). Phylogenetic analysis of these genes in *M. lupulina* and 20 genes of CNGCs in *Arabidopsis* (Zelman et al. 2012) showed that *c8828* is homologous with *AtCNGC2* (Supplementary Fig. S6a). In addition to *CNGC2*, *CNGC20* encoded by *c23173* (Supplementary Fig. S6a) was highly expressed in high calcium-treated leaves (Fig. 6b).

To maintain the intracellular Ca^{2+} homeostasis, excessive cytosolic Ca^{2+} needs to be transported into the intracellular calcium pool such as ER and vacuoles or extracellular spaces through Ca^{2+}-ATPases (ER-type Ca^{2+}-ATPase [ECA] and autoinhibited Ca^{2+}-ATPase [ACA]) and calcium exchangers (Bose et al. 2011; Conn et al. 2011; Sze et al. 2000). From our transcriptome data, six genes encoding Ca^{2+}-ATPase were identified and three (*c28999*, *c23420* and *c17993*) of these were found to be up-regulated by high calcium levels (Fig. 6c). Evolutionary analysis of these genes was shown in Supplementary Fig. S6b. Moreover, we identified an up-regulated gene *c26783* encoding the tonoplast-located Ca^{2+}/H^+

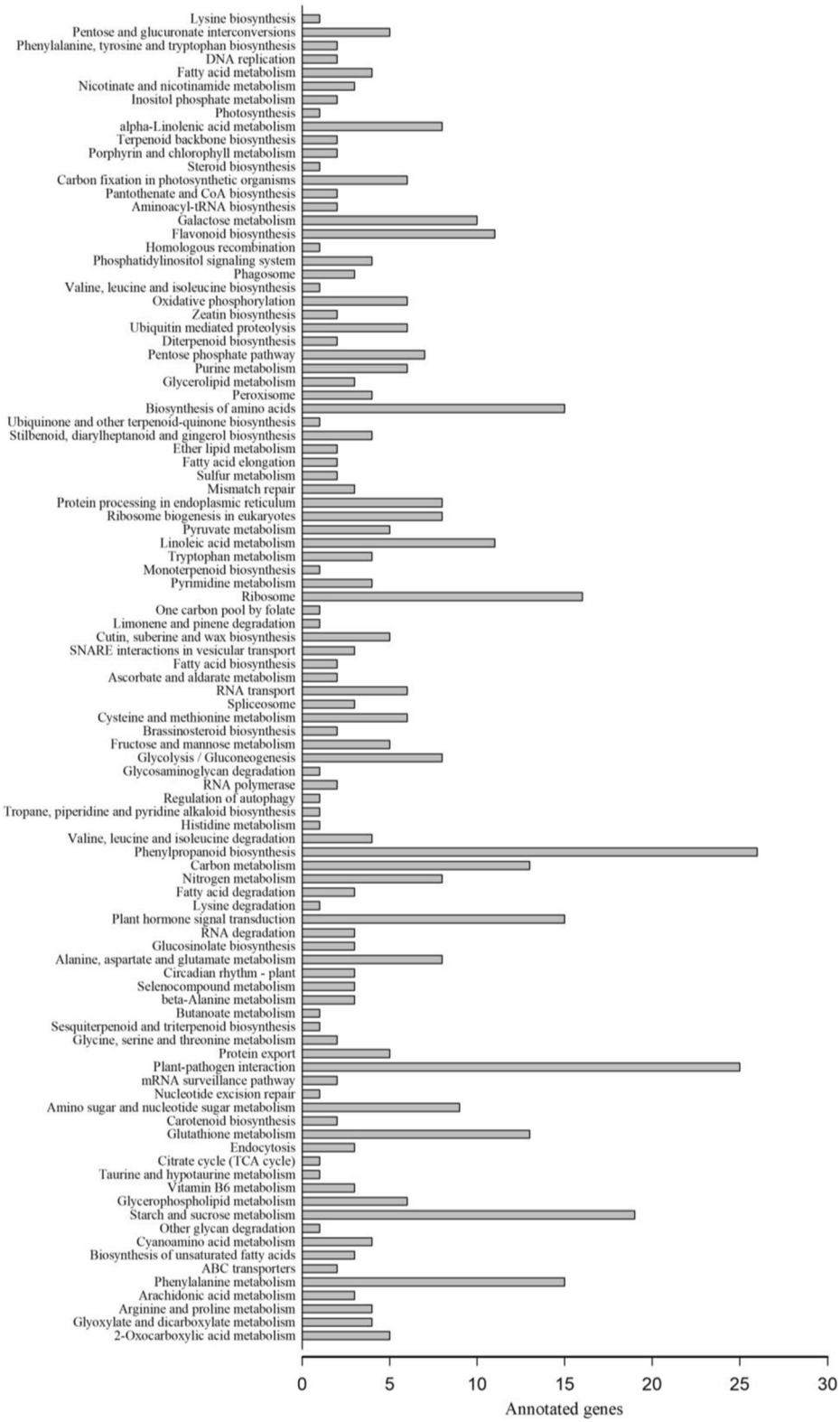

Fig. 4 KEGG pathway enrichment of differentially expressed genes (DEGs). X axis indicates the number of differentially expressed genes annotated to this pathway. Y axis indicates the name of the KEGG metabolic pathway

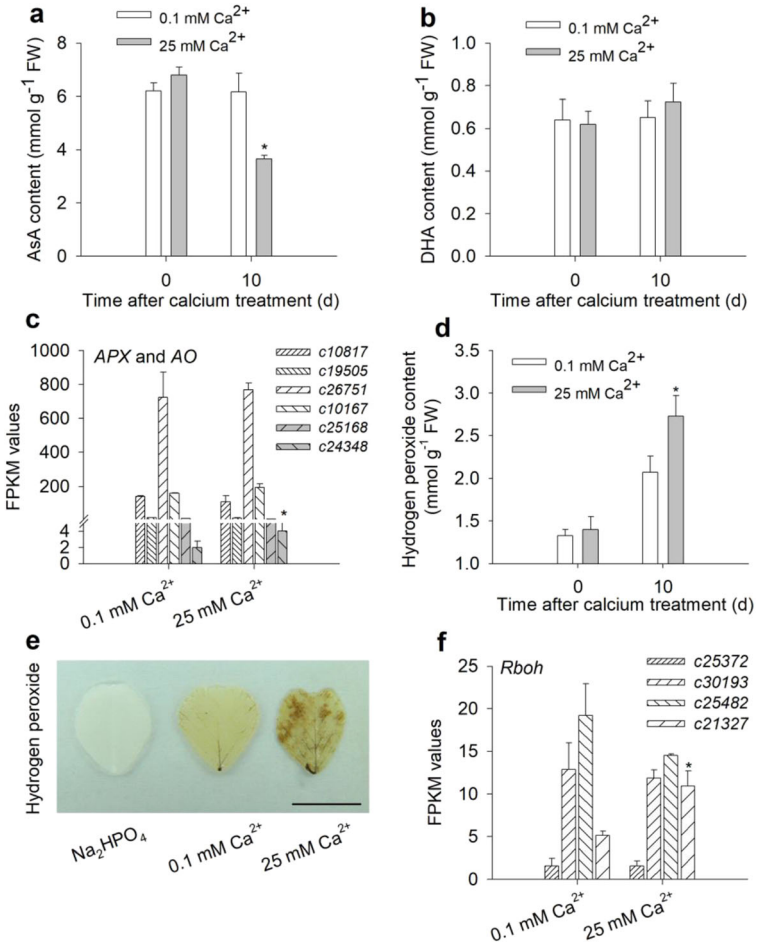

Fig. 5 AsA degradation, H_2O_2 production and related gene expression in calcium treated leaves of *M. lupulina*. **a** AsA content. **b** DHA content. **c** Genes encoding ascorbate peroxidase (*APX*, wihte) and ascorbate oxidase (*AO*, gray). **d** Hydrogen peroxide content. **e** Leaf hydrogen peroxide staining by DAB, bar = 1 cm. **f** Genes encoding respiratory burst oxidase homologues (*Rboh*). Data indicate mean ± standard deviation (SD) of three replicates and asterisk represents a significant difference between 0.1 mM Ca^{2+} and 25 mM Ca^{2+} treatment ($p < 0.05$)

transporters (CAX) that are involved in the calcium transport from the cytoplasm into the vacuoles (Fig. 6d). Further evolutionary analysis revealed that *c26783* is homologous with *AtCAX1* and *AtCAX3* (Supplementary Fig. S6c).

Furthermore, we identified two calcium-binding protein genes *c8929* encoding calreticulin (CRC) (Fig. 6e) and *c31492* encoding a CBP (Fig. 6f), both of which gent induced by a high concentration of calcium.

Discussion

Previous studies have reported that the accumulation of CaOx crystals in *Pistia stratiotes* and *Lemna minor* (Mazen et al. 2004; Volk et al. 2002) to be an extremely complicated process that involved oxalic acid biosynthesis, calcium transport and nucleation and growth of crystals. However, the literature on genes related to CaOx formation in plants has remained unclear. In the present study, we used transcriptome analysis to found 1322 genes to be up-regulated in leaves treated with 25 mM Ca^{2+} compared with leaves treated with 0.1 mM Ca^{2+}. Analyses of GO and KEGG pathways of the DEGs allowed the identification of genes related to AsA degradation, H_2O_2 production, and calcium transport in the leaves of CaOx-accumulating plant *M. lupulina* under high-calcium treatment. We aimed to understand the mechanism behind the biosynthesis of CaOx induced by high calcium.

Calcium availability induces calcium oxalate accumulation in *M. lupulina* leaves

Karst area is a famous for limestone karst topography, which is mainly composed of calcium carbonate. Soils, which were derived from limestone karst habitat, are characterized by high concentrations of calcium (Hao et al. 2015). High rhizospheric soluble calcium in this

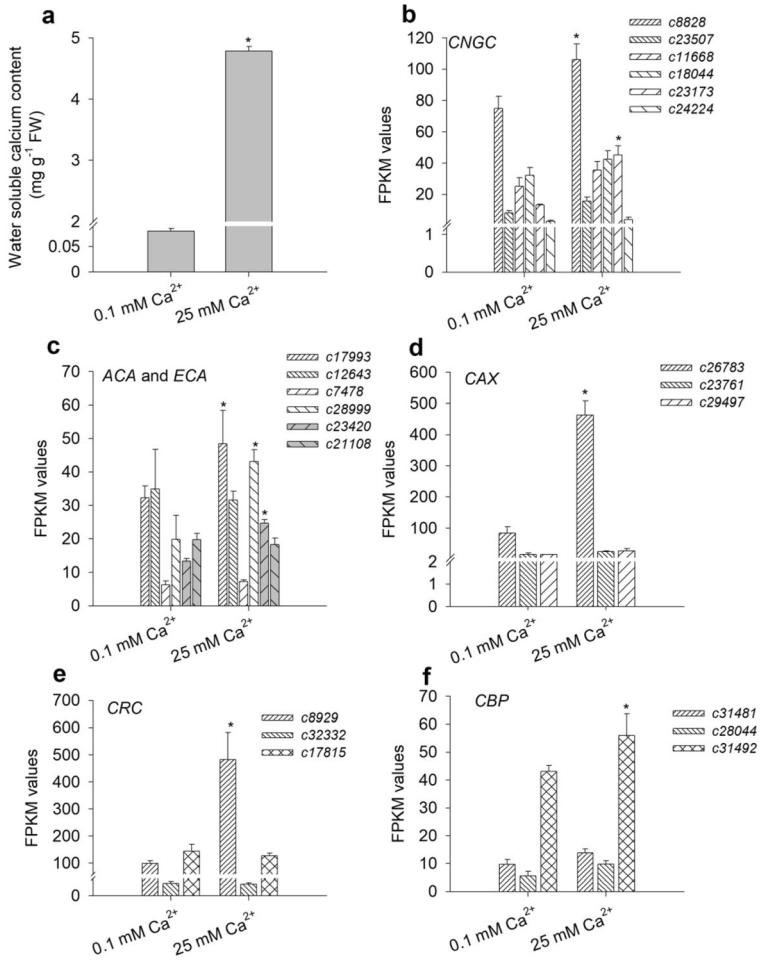

Fig. 6 Water-soluble calcium content and expression profiles of genes related to calcium transport and calcium binding proteins in high calcium treated leaves of *M. lupulina*. **a** Water-soluble calcium content in 0.1 and 25 mM Ca^{2+} treated leaves. **b** Cyclic nucleotide-gated channel genes (*CNGC*). **c** autoinhibited Ca^{2+}-ATPase (*ACA*, white) and ER-type Ca^{2+}-ATPase genes (*ECA*, gray). **d** Tonoplast-located Ca^{2+}/H^{+} transporters genes (*CAX*). **e** Calreticulin genes (CRC). **f** Calcium binding protein genes (CBP). Data indicate mean ± standard deviation (SD) of three replicates and asterisk represents a significant difference between 0.1 mM Ca^{2+} and 25 mM Ca^{2+} treatment ($p < 0.05$)

soil is one of the major factors that limit distribution and production of the species. However, some karst-adapted species (i.e., Fabaceae) can grow well in this habitat. It is known that most plants belong into Fabaceae display prismatic crystals in the leaf VBs and vein endings (Cervantes-Martinez et al. 2005; Nakata and Mcconn 2000; Nakata and Mcconn 2007). Three main calcium crystals, namely, calcium oxalate, calcium carbonate, and calcium sulfate, are reported to occur in plant tissues (He et al. 2014). However, FTIR spectroscopy and XRD techniques also employed by previous studies confirmed that the crystals in *M. lupulina* leaves mainly comprised CaOx (Supplementary Fig. S2) (Monje and Baran 2002). As expected, our results showed that the prismatic CaOx crystals (Fig. 1d) were present along the leaf VBs in CaOx-accumulating plant *M. lupulina* (Fig. 1e–h). The content of CaOx in the leaves increased significantly under high calcium treatment but not in roots and stems (Fig. 1a; Supplementary Fig. S1). The increase in the CaOx content in leaves could be attributed to the increase in the length of the crystals (Fig. 1a, c). It has been reported previously that CaOx crystal accumulation is induced by calcium availability in *P. stratiotes* and *L. minor* leaves (Mazen et al. 2004; Volk et al. 2002). The findings of our study suggested that exogenous calcium could also induce accumulation of CaOx crystals in *M. lupulina* leaves. The crystal formation among species is controlled by a combination of genetic and environmental factors (Franceschi et al. 1993; Mazen et al. 2004). Genetic factors need to be further studied to reveal the molecular mechanism of biosynthesis of CaOx among species.

Expression of genes related to calcium transport in response to calcium availability

It has been reported that *AtCNGC2* is primarily expressed in the leaf areas surrounding the free endings

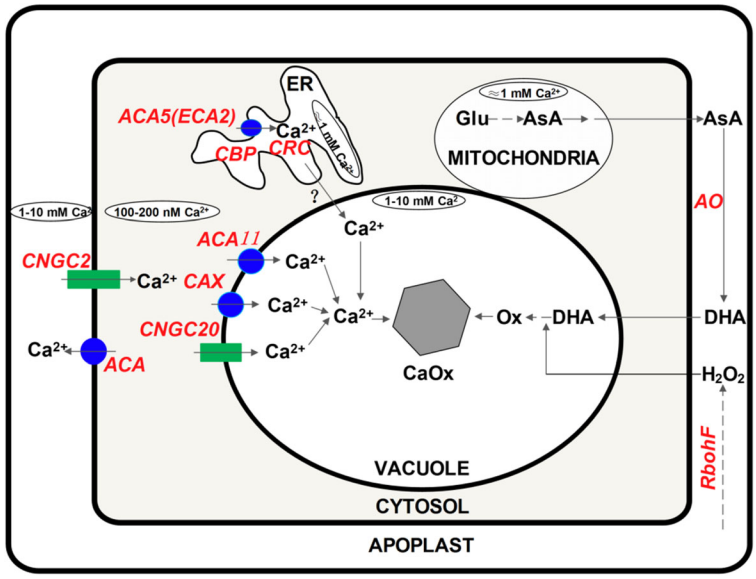

Fig. 7 Schematic diagram of CaOx formation in *M. lupulina* leaves under high calcium treatment. Calcium channels, Ca^{2+}-ATPase, H^+/Ca^{2+} exchanger, and ascorbate oxidase are involved in calcium transportation and oxalate biosynthesis. ACA, autoinhibited Ca^{2+}-ATPase; AO, ascorbate oxidase; CBP, calcium binding protein; AsA, ascorbate; CaOx, calcium oxalate crystals; CAX, vacuole H^+/Ca^{2+} exchanger; CNGC, cyclic nucleotide-gated channel; CRC, calreticulin; DHA, dehydroascorbate; ECA, ER-type Ca^{2+}-ATPase; ER, endoplasmic reticulum; Glu, glucose; Ox, oxalate. The red color represents an enzyme or a protein. The black color represents the reactant or product. The red bold indicates that the expressions of the genes are up-regulated

of minor veins and is responsible for transporting calcium into the cytoplasm (Smith et al. 2003; Wang et al. 2017). Our transcriptome data showed that the expression of *c8828* (homologous with *AtCNGC2*) (Fig. 6b and Supplementary Fig. S6a) induced by high calcium levels was consistent with the distribution of CaOx along the veins in *M. lupulina* leaves (Fig. 1e–h), suggesting that CNGC2 may play an important role in the transport of calcium for the synthesis of CaOx crystals in *M. lupulina*. Furthermore, the expression of *c23173* (homologous with *AtCNGC20*) induced by a high concentration of calcium may regulate its redistribution between the mesophyll and the vein cells, resulting in the entry of more calcium into the vein cells. This is consistent with a previous finding that reported *AtCNGC20* to be majorly located to the mesophyll cells surrounding the veins (Patricia et al. 2009).

Although *c28999* (homologous with *AtACA8*, *AtACA9*, and *AtACA10*) (Supplementary Fig. S6b) was induced in leaves treated with high concentration of calcium (Fig. 6c), it functions to regulate the efflux of Ca^{2+} into the extracellular spaces (Bose et al. 2011), which does not participate in the regulation of CaOx formation. However, it could play a central role in maintaining calcium homeostasis in the cytoplasm since high exogenous calcium treatment increased significantly water soluble-calcium content (Fig. 6a). In addition, the expression of *c23420* (encoding ER-located ECA2) was induced by high calcium levels (Fig. 6c and Supplementary Fig. S6b) that enhanced Ca^{2+} transport into the ER (Bose et al. 2011), where Ca^{2+} is bound to calreticulins and calcium binding proteins to buffer the cytoplasmic calcium (Franceschi and Nakata 2005). Our transcriptome data revealed the expression of genes encoding calreticulin and calcium binding protein to be up-regulated (Fig. 6e, f). This is considered to be an important regulatory step for formation of CaOx crystals (Franceschi et al. 1993; Kostman et al. 2003; Nakata et al. 2003). Furthermore, Ca^{2+} is sequestered from the cytosol into the vacuoles by tonoplast-located CAX and ACA11, resulting in a large amount of Ca^{2+} entering into the vacuoles (Martinoia et al. 2012; Pittman and Hirschi 2016; Wang et al. 2017). In the present study, the expression of *c17993* and *c26783* (encoding CAX and ACA11) was induced by a concentration of high calcium (Fig. 6c and d), suggesting that they were involved in the transport Ca^{2+} into the vacuoles for the formation of CaOx crystals. Moreover, the nucleation

and growth of crystals are regulated by matrix proteins within the vacuoles (Li et al. 2003; Nakata and Mcconn 2000). However, unfortunately, we could not identify any nucleation related genes from the transcriptome data.

Ascorbic acid degradation and hydrogen peroxide accumulation associated with calcium oxalate production

Our results revealed degradation of AsA (Fig. 5a) increased the content of CaOx (Fig.1a) in high calcium-treated *M. lupulina* leaves. This finding is consistent with that obtained in a previous study in *M. truncatula* mutants (Nakata and Mcconn 2007). Loewus and Franceschi (2001) reported AsA to be a precursor of insoluble oxalate biosynthesis. DHA acts as the intermediate product of AsA degradation to form oxalic acid (Parsons and Fry 2012). Theoretically, the DHA content should increase with AsA degradation; however, its content remained stable under low and high calcium treatments both at 0 day and ten days in *M. lupulina* leaves in the present study (Fig. 5b), suggesting the rapid oxidization of increased proportion of DHA to produce oxalic acid (Parsons et al. 2011).

Previous studies have reported AsA degradation to be catalyzed by H_2O_2 in vitro or in plant cell cultures (Parsons and Fry 2012; Parsons et al. 2011). The results presented in the current study revealed a high H_2O_2 accumulation in calcium-treated leaves (Fig. 5d and e) to be induced by calcium transported from the stem into the leaves through the apoplast pathway (White and Broadley 2003) and accumulated initially in the apoplastic space (Fig. 6a) (Wang et al. 2017). Further RNA sequencing indicated that the expression of respiratory burst oxidase homologous (Rboh) gene (*c21327*) that catalyzes H_2O_2 production in plants was up-regulated in high calcium-treated leaves (Fig. 5f), indicating Rboh to be involved in H_2O_2 accumulation, as reported previously in *Arabidopsis* under salt stress (Ben Rejeb et al. 2015; Ma et al. 2012) and in the guard cells in response to extracellular calcium (Wang et al. 2012).

Ascorbic acid acts as an antioxidant and plays an important role in oxidative stress (Fotopoulos et al. 2006). Although AsA is mainly distributed in the cytoplasm, a substantial proportion of it gets exported to the apoplastic space to create the first line of defense against oxidative stress (Fotopoulos et al. 2006; Pignocchi et al. 2006). Our transcriptome data analysis showed that the expression of gene encoding AO was up-regulated in high calcium-treated leaves, but not APX (Fig. 5c), suggesting the cell wall-localized AO and not APX to be more likely involved in AsA degradation in oxalate-accumulating *M. lupulina* leaves after high calcium treatment. This result provides direct evidence that the formation of oxalic acid from AsA is accelerated by AO and not by APX.

Conclusion

On the basis of the results of the present study, we propose a clear outline for the formation of CaOx in *M. lupulina* leaves under high calcium conditions (Fig. 7). Firstly, excessive water-soluble calcium gets transported to the leaves (Fig. 6a), where the H_2O_2 is produced via NADPH oxidase. Secondly, an up-regulated expression of ascorbate oxidase gene (*AO*) accelerates AsA degradation, whereas H_2O_2 enhances the accumulation of insoluble oxalic acid. Thirdly, the expression of genes related to calcium transport, including *CNGC2*, *CNGC20*, *ECA2*, and *CAX,* is significantly up-regulated under high calcium, resulting in Ca^{2+} transport into the vacuoles or ER. In ER, calcium could be bound to calreticulin or other calcium binding proteins to buffer the cytoplasmic calcium, which is an important regulatory step for the synthesis of CaOx crystals. Finally, CaOx was formed in the vacuoles with high levels of oxalic acid combined with high levels of calcium.

Acknowledgments This study was financially supported by the Joint Fund of the Natural Science Foundation of China and the Karst Science Research Center of Guizhou Province (Grant No. U1812401), the Programme for Changjiang Scholars and Innovative Research Teams in Universities (PCSIRT–1227), the Initial Fund for Key Laboratory of Guizhou Province (2011-4005), the Major Science and Technology Project of the Education Department of Guizhou Province during the "12th Five-year Plan" (2012-005), the Joint Fund for the Department of Science and Technology of Guizhou Province and Guizhou Normal University ([2016]7209, [2016]7210), the National Key Research and Development Program of China (2017YFC0506102), and the Natural Science Foundation of China (NSFC) (31570586, 31870581).

Author contributions X. M. Z. designed the experiments. X. M. Z., L. X. L. and Z. M. S performed the experiments. Z. J. S. and G. F. G. analyzed transcriptome data. X. M. Z. wrote the paper. Y.

Y. and H. L. Z. revised this paper. All authors have read and approved the manuscript.

Compliance with ethical standards

Competing financial interests We declare no competing financial interests.

References

Ashburner M, Ball CA, Blake JA, Botstein D, Butler H, Cherry JM, Davis AP, Dolinski K, Dwight SS, Eppig JT, Harris MA, Hill DP, Issel-Tarver L, Kasarskis A, Lewis S, Matese JC, Richardson JE, Ringwald M, Rubin GM, Sherlock G (2000) Gene ontology: tool for the unification of biology. The gene ontology consortium. Nat Genet 25:25–29

Bafeel SO, Ibrahim MM (2008) Antioxidants and accumulation of α-tocopherol induce chilling tolerance in *Medicago sativa*. Int J Agric Biol 10:1560–8530

Ben Rejeb K, Lefebvre-De Vos D, Disquet IL, Leprince AS, Bordenave M, Maldiney R, Jdey A, Abdelly C, Savouré A (2015) Hydrogen peroxide produced by NADPH oxidases increases proline accumulation during salt or mannitol stress in *Arabidopsis thaliana*. New Phytol 208:1138–1148

Bose J, Pottosin II, Shabala SS, Palmgren MG, Shabala S (2011) Calcium efflux systems in stress signaling and adaptation in plants. Front Plant Sci 85:1–17

Cervantes-Martinez T, Horner HT, Palmer RG, Hymowitz T, Ahd B (2005) Calcium oxalate crystal macropatterns in leaves of species from groups *Glycine* and *Shuteria* (Glycininae; Phaseoleae; Papilionoideae; Fabaceae). Can J Bot 83:1410–1421

Conn SJ, Gilliham M, Athman A, Schreiber AW, Baumann U, Moller I, Cheng NH, Stancombe MA, Hirschi KD, Webb AA (2011) Cell-specific vacuolar calcium storage mediated by CAX1 regulates apoplastic calcium concentration, gas exchange, and plant productivity in *Arabidopsis*. Plant Cell 23: 240–257

Daudi A, Cheng Z, O'Brien JA, Mammarella N, Khan S, Ausubel FM, Bolwell GP (2012) The apoplastic oxidative burst peroxidase in *Arabidopsis* is a major component of pattern-triggered immunity. Plant Cell 24:275–287

Fotopoulos V, Sanmartin M, Kanellis AK (2006) Effect of ascorbate oxidase over-expression on ascorbate recycling gene expression in response to agents imposing oxidative stress. J Exp Bot 57:3933–3943

Franceschi VR (1989) Calcium oxalate formation is a rapid and reversible process in *Lemna minor* L. Protoplasma 148:130–137

Franceschi VR (2001) Calcium oxalate in plants. Trends Plant Sci 6:331–331

Franceschi VR, Nakata PA (2005) Calcium oxalate in plants: formation and function. Annu Rev Plant Biol 56:41–71

Franceschi VR, Li X, Zhang DZ, Okita TW (1993) Calsequestrinlike calcium-binding protein is expressed in calcium-accumulating cells of *Fistia stratiotes*. Proc Natl Acad Sci 90:6986–6990

Gallaher RN (1975) The occurrence of calcium in plant tissue as crystals of calcium oxalate. Commun Soil Sci Plant Anal 6: 315–330

Grabherr MG, Haas BJ, Yassour M, Levin JZ, Thompson DA, Amit I, Xian A, Fan L, Raychowdhury R, Zeng Q (2011) Trinity: reconstructing a full-length transcriptome without a genome from RNA-Seq data. Nat Biotechnol 29:644–652

Green MA, Fry SC (2005) Vitamin C degradation in plant cells via enzymatic hydrolysis of 4-O-oxalyl-L-threonate. Nature 433: 83–87

Hao Z, Kuang Y, Kang M, Niu S (2015) Untangling the influence of phylogeny, soil and climate on leaf element concentrations in a biodiversity hotspot. Funct Ecol 29:165–176

He H, Veneklaas EJ, Kuo J, Lambers H (2014) Physiological and ecological significance of biomineralization in plants. Trends Plant Sci 19:166–174

Horner HT, Wagner BL (1995) Calcium oxalate formation in higher plants. In: Khan S (ed) Calcium oxalate in biological systems. CRC Press, Boca Raton, pp 53–72

Horner HT, Kausch AP, Wagner BL (2000) Ascorbic acid: a precursor of oxalate in crystal idioblasts of *Yucca torreyi* in liquid root culture. Int J Plant Sci 161(6):861–868

Horner HT, Wanke S, Samain MS (2012) A comparison of leaf crystal macropatterns in the two sister genera *Piper* and *Peperomia* (Piperaceae). Am J Bot 99:983–997

Joshi S, Wang W, Peck A, Khan S, Gainesville FL (2013) Differential gene expression in rat kidneys in response to oxalate and calcium oxalate crystals: a transcriptional study. J Urol 189:e854–e855

Joshi S, Wang W, Khan SR (2017) Transcriptional study of hyperoxaluria and calcium oxalate nephrolithiasis in male rats: inflammatory changes are mainly associated with crystal deposition. PLoS One 12:1–21

Kausch AP, Horner HT (1985) Absence of $CeCl_3$-detectable peroxisomal glycolate-oxidase activity in developing raphide crystal idioblasts in leaves of *Psychotria punctata* Vatke and roots of *Yucca torreyi* L. Planta 164:35–43

Keates SE, Tarlyn NM, Loewus FA, Franceschi VR (2000) L-ascorbic acid and L-galactose are sources for oxalic acid and calcium oxalate in *Pistia stratiotes*. Phytochem 53:433–440

Km G, Ea A (2007) Measurement of reduced, oxidized and total ascorbate content in plants. Nat Protoc 2:871–874

Kostman TA, Tarlyn NM, Loewus FA, Franceschi VR (2001) Biosynthesis of L-ascorbic acid and conversion of carbons 1 and 2 of L-ascorbic acid to oxalic acid occurs within individual calcium oxalate crystal idioblasts. Plant Physiol 125:634–640

Kostman TA, Franceschi VR, Nakata PA (2003) Endoplasmic reticulum sub-compartments are involved in calcium sequestration within raphide crystal idioblasts of *Pistia stratiotes*. Plant Sci 165:205–212

Lersten NR, Horner HT (2009) Crystal diversity and macropatterns in leaves of Oleaceae. Plant Syst Evol 282: 87–102

Li X, Zhang D, Lynch-Holm VJ, Okita TW, Franceschi VR (2003) Isolation of a crystal matrix protein associated with calcium

oxalate precipitation in vacuoles of specialized cells. Plant Physiol 133:549–559
Libert B, Franceschi VR (1987) Oxalate in crop plants. J Agric Food Chem 35:926–938
Livak KJ, Schmittgen TD (2012) Analysis of relative gene expression data using real-time quantitative PCR and the 2(−Delta Delta C(T)) method. Methods 25:402–408
Loewus FA, Franceschi VR (2001) Biosynthesis of L-ascorbic acid and conversion of carbons 1 and 2 of L-ascorbic acid to oxalic acid occurs within individual calcium oxalate crystal idioblasts. Plant Physiol 125:634–640
Ma L, Zhang H, Sun L, Jiao Y, Zhang G, Miao C, Hao F (2012) NADPH oxidase *AtrbohD* and *AtrbohF* function in ROS-dependent regulation of Na^+/K^+ homeostasis in *Arabidopsis* under salt stress. J Exp Bot 63:305–317
Martinoia E, Meyer S, Angeli AD, Nagy R (2012) Vacuolar transporters in their physiological context. Annu Rev Plant Biol 63:183–213
Mazen AMA, Zhang D, Franceschi VR (2004) Calcium oxalate formation in *Lemna minor*: physiological and ultrastructural aspects of high capacity calcium sequestration. New Phytol 161:435–448
Mcconn MM, Nakata PA (2002) Calcium oxalate crystal morphology mutants from *Medicago truncatula*. Planta 215:380–386
Minocha R, Chamberlain B, Long S, Turlapati SA, Quigley G (2015) Extraction and estimation of the quantity of calcium oxalate crystals in the foliage of conifer and hardwood trees. Tree Physiol 35:574–580
Minoru K, Susumu G, Shuichi K, Yasushi O, Masahiro H (2004) The KEGG resource for deciphering the genome. Nucleic Acids Res 32:D277–D280
Monje PV, Baran EJ (2002) Characterization of calcium oxalates generated as biominerals in cacti. Plant Physiol 128:707–713
Nakata PA (2003) Advances in our understanding of calcium oxalate crystal formation and function in plants. Plant Sci 164:901–909
Nakata PA (2012) Engineering calcium oxalate crystal formation in Arabidopsis. Plant Cell Physiol 53:1275–1282
Nakata PA, Mcconn MM (2000) Isolation of *Medicago truncatula* mutants defective in calcium oxalate crystal formation. Plant Physiol 124:1097–1104
Nakata PA, Mcconn MM (2003) Influence of the calcium oxalate defective 4 (cod4) mutation on the growth, oxalate content, and calcium content of *Medicago truncatula*. Plant Sci 164: 617–621
Nakata PA, Mcconn MM (2007) Genetic evidence for differences in the pathways of druse and prismatic calcium oxalate crystal formation in *Medicago truncatula*. Funct Plant Biol 34:332–338
Nakata PA, Kostman TA, Franceschi VR (2003) Calreticulin is enriched in the crystal idioblasts of *Pistia stratiotes*. Plant Physiol Biochem 41:425–430
Nuss RF, Loewus FA (1978) Further studies on oxalic acid biosynthesis in oxalate-accumulating plants. Plant Physiol 61: 590–592
Okada A, Yasui T, Hamanoto S, Hirose M, Kubota Y, Itoh Y, Tozawa K, Hayashi Y, Kohri K (2010) Genome-wide analysis of genes related to kidney stone formation and elimination in the calcium oxalate nephrolithiasis model mouse: detection of stone-preventive factors and involvement of macrophage activity. J Bone Miner Res 24:908–924
Parsons HT, Fry SC (2012) Oxidation of dehydroascorbic acid and 2,3-diketogulonate under plant apoplastic conditions. Phytochem 75:41–49
Parsons HT, Yasmin T, Fry SC (2011) Alternative pathways of dehydroascorbic acid degradation in vitro and in plant cell cultures: novel insights into vitamin C catabolism. Biochem J 440:375–383
Patricia W, Klaus P, Barbara K, Annette K, Petra D (2009) Salt-dependent regulation of a CNGC channel subfamily in *Arabidopsis*. BMC Plant Biol 9:1–11
Pierantoni M, Tenne R, Rephael B, Brumfeld V, Van AC, Kupczik K, Oron D, Addadi L, Weiner S (2018) Mineral deposits in ficus leaves: morphologies and locations in relation to function. Plant Physiol 176:1751–1763
Pignocchi C, Kiddle G, Hernández I, Foster SJ, Asensi A, Taybi T, Barnes J, Foyer CH (2006) Ascorbate oxidase-dependent changes in the redox state of the apoplast modulate gene transcript accumulation leading to modified hormone signaling and orchestration of defense processes in tobacco. Plant Physiol 141:423–435
Pittman JK, Hirschi KD (2016) CAX-ing a wide net: cation/H^+ transporters in metal remediation and abiotic stress signalling. Plant Biol 18:741–749
Pruitt KD, Tatusova T, Maglott DR (2005) NCBI reference sequence (RefSeq): a curated non-redundant sequence database of genomes, transcripts and proteins. Nucleic Acids Res 33: D501–D504
Smith RK, Bent AF, Sussman MR (2003) A cyclic nucleotide-gated ion channel, CNGC2, is crucial for plant development and adaptation to calcium stress. Plant Physiol 132:728–731
Sun YL, Zhang DH, Zhao L, Xia CC, Min-Xia C (2014) Reference gene selection for real-time quantitative PCR in black medic (*Medicago lupulina* L.) root tissue under copper stress. J Agricul Biotechnol 22:1223–1231
Sze H, Liang F, Hwang I, Curran AC, Harper JF (2000) Diversity and regulation of plant Ca^{2+} pumps: insights from expression in yeast. Annu Rev Plant Biol 51:433–462
Tatusov RL, Galperin MY, Natale DA, Koonin EV (2000) The COG database: a tool for genome-scale analysis of protein functions and evolution. Nucleic Acids Res 28:33–36
Tooulakou G, Giannopoulos A, Nikolopoulos D, Bresta P, Dotsika E, Orkoula MG, Kontoyannis CG, Fasseas C, Liakopoulos G, Klapa MI (2016) Alarm photosynthesis: calcium oxalate crystals as an internal CO_2 source in plants. Plant Physiol 171:2577–2585
Trapnell C, Williams BA, Pertea G, Mortazavi A, Kwan G, van Baren MJ, Salzberg SL, Wold BJ, Pachter L (2010) Transcript assembly and quantification by RNA-Seq reveals unannotated transcripts and isoform switching during cell differentiation. Nat Biotechnol 28:511–515
Truffault V, Fry SC, Stevens RG, Gautier H (2016) Ascorbate degradation in tomato leads to accumulation of oxalate, threonate and oxalyl threonate. Plant J 89:996–1008
Volk GM, Lynch-Holm VJ, Kostman TA, Goss LJ, Franceschi VR (2002) The role of druse and raphide calcium oxalate crystals in tissue calcium regulation in *Pistia stratiotes* leaves. Plant Biol 4:34–45
Volk GM, Goss LJ, Franceschi VR (2004) Calcium channels are involved in calcium oxalate crystal formation in specialized cells of *Pistia stratiotes* L. Ann Bot 93:741–753

Wang WH, Yi XQ, Han AD, Liu TW, Chen J, Wu FH, Dong XJ, He JX, Pei ZM, Zheng HL (2012) Calcium-sensing receptor regulates stomatal closure through hydrogen peroxide and nitric oxide in response to extracellular calcium in *Arabidopsis*. J Exp Bot 63:177–190

Wang Y, Kang Y, Ma C, Miao R, Wu C, Long Y, Ge T, Wu Z, Hou X, Zhang J, Qi Z (2017) CNGC2 is a Ca^{2+} influx channel that prevents accumulation of apoplastic Ca^{2+} in the leaf. Plant Physiol 173:1342–1354

Webb MA (1999) Cell-mediated crystallization of calcium oxalate in plants. Plant Cell 11:751–761

Webb MA, Cavaletto JM, Carpita NC, Lopez LE, Arnott HJ (1995) The intravacuolar organic matrix associated with calcium oxalate crystals in leaves of Vitis. Plant J 7:633–648

White PJ, Broadley MR (2003) Calcium in plants. Ann Bot 92: 487–511

Yu L, Jiang J, Zhang C, Jiang L, Ye N, Lu Y, Yang G, Liu E, Peng C, He Z, Peng X (2010) Glyoxylate rather than ascorbate is an efficient precursor for oxalate biosynthesis in rice. J Exp Bot 61:1625–1634

Zelman AK, Dawe A, Gehring C, Berkowitz GA (2012) Evolutionary and structural perspectives of plant cyclic nucleotide-gated cation channels. Front Plant Sci 3:1–13